ATMOSPHERIC SCIENCE LETTERS
Atmos. Sci. Let. **18**: 175–182 (2017)
Published online in Wiley Online Library
(wileyonlinelibrary.com) **DOI:** 10.1002/asl.740

RMetS
Royal Meteorological Society

Revisiting the relationship between the South Asian summer monsoon drought and El Niño warming pattern

Fangxing Fan,[1]* Xiao Dong,[1] Xianghui Fang,[2] Feng Xue,[1] Fei Zheng[1] and Jiang Zhu[1]

[1]*International Center for Climate and Environment Sciences, Institute of Atmospheric Physics, Chinese Academy of Sciences, Beijing, China*
[2]*Institute of Atmospheric Sciences, Fudan University, Shanghai, China*

**Correspondence to:*
F. Fan, International Center for Climate and Environment Sciences, Institute of Atmospheric Physics, Chinese Academy of Sciences, Beijing 100029, China.
E-mail: fanfangxing@mail.iap.ac.cn

Received: 6 May 2016
Revised: 18 December 2016
Accepted: 2 February 2017

Abstract

Based on the observational and reanalysis data, El Niño warming patterns associated with the South Asian summer monsoon droughts are investigated. While the inverse relationship between the eastern Pacific (EP) type of El Niño-Southern Oscillation (ENSO) and the Indian monsoon rainfall weakened significantly, the correlation between the central Pacific (CP) type of ENSO and the monsoon rainfall strengthened after the late 1970s. Moreover, the drought-producing El Niño warming pattern also exhibits a notable decadal modulation associated with the climate shift. The analysis results indicate that both the EP type of El Niño with positive sea surface temperature (SST) anomalies extended to the date line and the CP type of El Niño with the maximum warming located in the central equatorial Pacific may produce severe droughts over the Indian subcontinent. Although the CP warming is more effective in driving anomalous rising motion in the central equatorial Pacific and consequently producing anomalous subsidence over South Asia, the position and strength of the anomalous ascending and descending branches of the Walker circulation are sensitive to the detailed distributions of tropical SST anomalies and determined by the competing effects of the CP and EP warming.

Keywords: **South Asian summer monsoon; eastern Pacific El Niño; central Pacific El Niño; El Niño warming pattern; decadal transition**

1. Introduction

El Niño-Southern Oscillation (ENSO) is the dominant mode of climate variability on interannual timescale, which can exert great impacts on the global climate, including the South Asian summer monsoon (SASM). The relationship between ENSO and SASM on both interannual and interdecadal timescales has been extensively addressed by many previous studies (Rasmusson and Carpenter, 1983; Ropelewski and Halpert, 1987; Webster and Yang, 1992; Grove, 1998; Krishnamurthy and Goswami, 2000; Fan *et al.,* 2010). The warm (cold) episodes of ENSO tend to be associated with below-normal (above-normal) Indian monsoon rainfall, and the El Niño index and the All-India monsoon rainfall (AIMR) index (Mooley and Parthasarathy, 1984; Parthasarathy *et al.,* 1994) are significantly and negatively correlated. The recognition of a different type of El Niño, referred to as the central Pacific (CP) El Niño (Ashok *et al.,* 2007; Yu and Kao, 2007; Ashok and Yamagata, 2009; Kao and Yu, 2009; Kug *et al.,* 2009), provides a new way to explore ENSO influences on global and regional climate. Different from the canonical eastern Pacific (EP) El Niño, the CP type of El Niño is characterized by positive sea surface temperature (SST) anomalies concentrated in the central tropical Pacific and is less sensitive to the thermocline variations (Kao and Yu, 2009; Zheng *et al.,* 2014). As the ENSO affects the SASM through the east–west displacement of the Walker circulation, the change in spatial configurations of SST anomalies leads to the change in the position and strength of the rising and sinking branches of the Walker circulation anomalies, and consequently alters the spatial distributions of precipitation anomalies over South and Southeast Asia (Ropelewski and Halpert, 1987; Palmer *et al.,* 1992).

The climate system experienced notable decadal variation in the late 1970s, which is related to the phase transition of the Pacific Decadal Oscillation (Trenberth, 1990; Mantua and Hare, 2002) and human activity induced global warming. During this climate transition, the conventional inverse relationship between ENSO and SASM has collapsed. Krishna Kumar *et al.* (1999) analyzed the 140-year historical record and found a drop in correlations between Indian summer monsoon rainfall and summer (June-July-August (JJA) mean) Niño-3 SST anomalies after the late 1970s. Although this weakening of the ENSO-Indian monsoon rainfall relationship may be due to natural variability (Mehta and Lau, 1997; Gershunov *et al.,* 2001), some evidence (Krishna Kumar *et al.,* 1999) suggests that anthropogenic global warming might be the root cause. Further investigations (Krishna Kumar *et al.,* 2006) of the detailed spatial distributions of eastern-to-central tropical Pacific SST anomalies related to the Indian monsoon droughts revealed that

El Niño events characterized by CP warming are more effective in producing Indian monsoon failure than those accompanied by EP warming.

Better understanding of the ENSO-monsoon association is of great importance for monsoon predictions. The precipitation data used in Krishna Kumar *et al.* (2006) to illustrate composite spatial patterns only covers the period 1979–2004. Whether the Indian monsoon drought-related El Niño warming pattern underwent a decadal shift is still unclear. The objectives of this study are to identify the spatial characteristics of El Niño warming patterns associated with the Indian monsoon droughts and to examine whether the monsoon drought-inducing El Niños exhibit different warming patterns between pre- and post-late 1970s. The rest of this article is organized as follows. The data and method are described in Section 2. Section 3 shows the main results, followed by conclusions in Section 4.

2. Data and method description

The observational data used in this study include monthly mean SST data provided by the Hadley Centre's sea ice and sea surface temperature dataset (HadISST) (Rayner *et al.,* 2003) and the precipitation dataset with high-resolution grids for Asia developed by the Asian Precipitation – Highly Resolved Observational Data Integration Towards Evaluation of Water Resources (APHRODITE) project (Yatagai *et al.,* 2012). The APHRODITE's precipitation dataset has been used to evaluate the models' performance in reproducing observed precipitation in East Asia (Lin and Zhou, 2015). This study also used precipitation and velocity potential from the Twentieth Century Reanalysis Version 2 (Compo *et al.,* 2011), which was provided by the National Oceanic and Atmospheric Administration's (NOAA's) Office of Oceanic and Atmospheric Research (OAR) Earth System Research Laboratory (ESRL) Physical Science Division (PSD), Boulder, Colorado, from its website (http://www.esrl.noaa.gov/psd/). This long-term reanalysis dataset was generated using an Ensemble Kalman Filter data assimilation method and surface pressure observations were assimilated into the model.

The AIMR, representing the interannual variability of the regionally averaged summer monsoon [June–September (JJAS)] rainfall over India, was calculated based on rain gauge observations from hundreds of stations (Parthasarathy *et al.,* 1995). While the influence of ENSO on the East Asian summer monsoon is significant during the decaying stage of ENSO through an anomalous western North Pacific anticyclone (Wang *et al.,* 2000), the ENSO has an instantaneous impact on the SASM in the developing phase of ENSO by altering the ascending and descending branches of the Walker circulation (Krishna Kumar *et al.,* 1999; Wang *et al.,* 2001). The criterion for selecting strong El Niño events is that the standardized boreal summer mean (JJAS) Niño-3 (5°S–5°N, 90–150°W) SST anomaly index is greater than +1.0. It is worth noting that we have used the summer rather than winter Niño-3 index in this study to identify El Niño events because we focus on examining the simultaneous relationship between ENSO and SASM. Furthermore, the EP and CP types of El Niño have been differentiated using a previously derived procedure [i.e. the combined regression-Empirical Orthogonal Function (EOF) method] (Kao and Yu, 2009; Yu *et al.,* 2012). To define the EP ENSO index, the SST anomalies regressed on the Niño-4 (5°S–5°N, 160°E–150°W) index were firstly removed from the original SST anomalies, and then the leading principal component of the residual SST anomalies was extracted with the EOF analysis to represent the EP ENSO variability. Similarly, the CP ENSO index was defined as the leading principal

Table 1. Strong El Niño events (standardized Niño-3 index > 1.0) and the associated All-India monsoon rainfall (AIMR) during the shorter (1950–2012) and longer (1871–2012) periods.

Years	Niño-3 SST anomaly (°C)	Standardized Niño-3 SST anomaly index	Type	AIMR (mm)	Standardized AIMR index
Strong El Niño events (1950–2012)					
1951	1.11	1.46	EP	738.7	−1.20
1957	1.18	1.55	EP	788.5	−0.61
1963	0.86	1.13	CP	857.7	0.21
1965	1.22	1.60	EP	709.2	−1.54
1972	1.62	2.12	EP	652.8	−2.21
1976	0.96	1.26	EP	856.6	0.20
1982	1.19	1.56	EP	735.1	−1.24
1983	1.03	1.35	EP	955.6	1.37
1987	1.43	1.88	CP	697.0	−1.69
1997	2.40	3.15	EP	871.4	0.37
Strong El Niño Events (1871–2012)					
1877	1.63	2.42	CP	603.9	−2.93
1888	0.98	1.46	EP	811.4	−0.44
1896	0.82	1.22	EP	828.4	−0.23
1900	0.84	1.25	CP	889.2	0.50
1902	1.45	2.16	CP	791.7	−0.67
1904	0.72	1.08	EP	750.1	−1.17
1905	1.27	1.88	CP	716.3	−1.58
1914	0.80	1.19	EP	897.9	0.60
1918	0.85	1.27	EP	650.6	−2.37
1919	0.74	1.10	CP	884.4	0.44
1925	0.87	1.30	EP	803.5	−0.53
1930	0.97	1.44	EP	804.4	−0.52
1941	0.76	1.13	CP	728.1	−1.44
1951	1.01	1.50	EP	738.7	−1.31
1957	1.09	1.62	EP	788.5	−0.71
1963	0.79	1.17	EP	857.7	0.12
1965	1.16	1.71	EP	709.2	−1.66
1972	1.58	2.34	EP	652.8	−2.34
1976	0.94	1.39	EP	856.6	0.10
1982	1.18	1.75	EP	735.1	−1.35
1983	1.03	1.52	EP	955.6	1.29
1987	1.44	2.13	CP	697.0	−1.81
1997	2.44	3.62	EP	871.4	0.28
2009	0.79	1.18	CP	667.6	−2.16

The EP and CP types of El Niño are identified based on the EP/CP ENSO index method developed by Kao and Yu (2009).

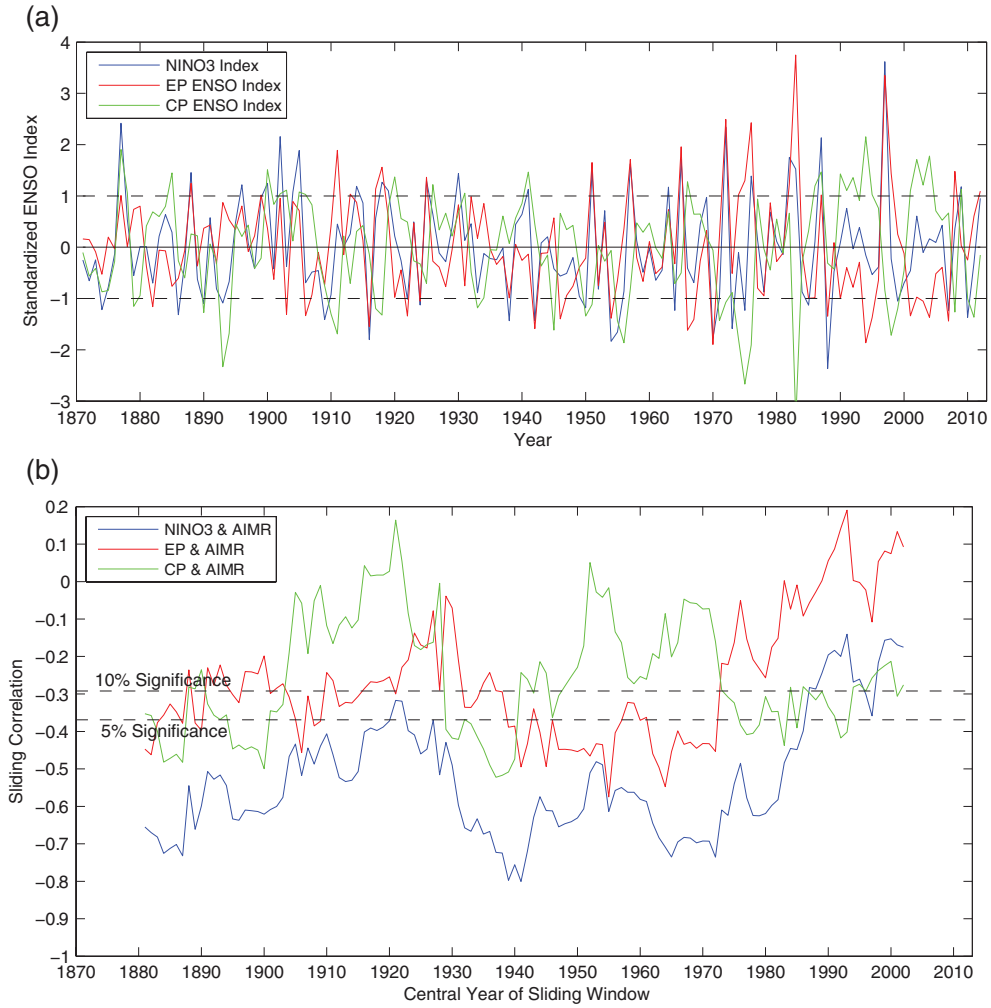

Figure 1. (a) Interannual time series of the Niño-3 SST anomaly index (blue), the EP ENSO index (red), and the CP ENSO index (green) for boreal summer season (June–September) during the 1871–2012 period. These series have been standardized to have zero mean and unit standard deviation. (b) Sliding correlations on a 21-year moving window between the ENSO indices and the AIMR index during the 1871–2012 period. The horizontal dashed lines indicate the one-tailed $p = 0.05$ and $p = 0.1$ significance levels.

component of the SST anomalies in which the influence from the Niño 1 + 2 (0–10°S, 80–90°W) region had been removed. Strong El Niño events were classified into EP and CP types based on the relative values of the summer mean EP and CP ENSO indices. The selected strong El Niño events and two types of El Niño during two time periods are listed in Table 1.

3. Results

The interannual variations of the standardized summer mean (JJAS) Niño-3 SST anomaly index and the two types of ENSO indices are shown in Figure 1(a). The Niño-3 index is highly correlated with the EP ENSO index ($r = 0.66$) and weakly but significantly correlated with the CP ENSO index ($r = 0.21$) during the 1871–2012 period. Figure 1(b) illustrates the sliding correlations on a 21-year moving window between the ENSO indices and the AIMR index. The sliding correlations between the Niño-3 index and the AIMR index were substantially significant before the 1980s but weakened considerably thereafter. The sliding correlations between the EP ENSO index and the AIMR index, though relatively weak, are almost in phase with those between the Niño-3 index and the AIMR index. The in-phase oscillations of the two sliding correlation curves imply that the weakening of the ENSO-SASM relationship after the late 1970s may be partly explained by the breakdown in the connection between the EP ENSO and the Indian monsoon rainfall. By contrast, the sliding correlations between the CP ENSO index and the AIMR index strengthened ($r = -0.3 \sim -0.4$) and became marginally significant ($p < 0.1$) in the last three decades of the twentieth century, indicating that the CP type of SST variation could explain $9 \sim 16\%$ of the Indian monsoon rainfall variability during this time interval. It should be noted that the SASM response to CP El Niño warming is sensitive to the specific definition of the CP ENSO index (Garfinkel *et al.*, 2013).

Figure 2 shows the simultaneous relationship between Niño-3 SST anomalies and the Indian monsoon rainfall anomalies in boreal summer season. It is evident

that deficient (abundant) Indian monsoon rainfall conditions are more likely to occur in the developing phase of El Niño (La Niña) events. The negative correlations between the Niño-3 index and the AIMR index are statistically significant at the one-tailed $p = 0.001$ level for both the shorter 1950–2012 interval ($r = -0.48$) and longer 1871–2012 interval ($r = -0.53$). However, the occurrence of moderate to strong El Niño events does not necessarily guarantee the Indian monsoon failure. For 10 (24) strong El Niño events (standardized Niño-3 index > 1.0) during the 1950–2012 period (the 1871–2012 period), only half of them produced Indian monsoon droughts (standardized AIMR index < −1.0), whereas the other half were accompanied by normal (−1.0 ≤ standardized AIMR index ≤ 1.0) or even abundant rainfall (standardized AIMR index > 1.0) conditions. Given the important role of the CP warming in the Indian monsoon drought raised by Krishna Kumar *et al.* (2006), it is worth asking whether the drought-inducing El Niños are of the CP type. Somewhat surprisingly, for the shorter 1950–2012 period (Figure 2(a)), there is not a clear split between the EP and CP types of strong El Niños with respect to this consideration. When the time interval is extended back to 1871 (Figure 2(b)), we found a greater tendency for the CP El Niños (62.5%; 5 out of 8) to produce Indian monsoon droughts than the EP El Niños (37.5%; 6 out of 16). However, because of the difficulty in discerning El Niño types from the early record when data are sparse (Giese and Ray, 2011), these results are not sufficient to demonstrate that the CP type of El Niño is the determinative factor in the Indian monsoon failure.

We next examined the differences in composite spatial patterns of SST and precipitation between drought (standardized AIMR index < −1.0) and drought-free (standardized AIMR index ≥ −1.0) El Niño years (Figure 3). Undoubtedly, the composite difference patterns of precipitation are featured by substantially decreased rainfall over the Indian subcontinent (Figure 3(a)). During the 1950–2012 period, the primary differences in composite SST pattern are the greater warming in the central Pacific around 170°W and less warming in the eastern Pacific along the South American coast, consistent with the results in Krishna Kumar *et al.* (2006). Splitting the whole period (1950–2012) into two subperiods (i.e. pre-1979 and post-1979), we found that the composite SST difference patterns corresponding to the drought *versus* drought-free rainfall conditions exhibit contrasting features (Figure 3(b)). The composite SST difference pattern in the later subperiod is quite similar to that in the whole period, though the positive and negative SST anomalies in the central and eastern Pacific are more significant. In contrast, the drought-inducing El Niño pattern in the earlier subperiod is characterized by overall enhanced warming in both central and eastern equatorial Pacific, and the most prominent enhancement of warming appears in the Niño1 + 2 region. Similar composite difference patterns can also be produced by a larger group of El Niño events selected

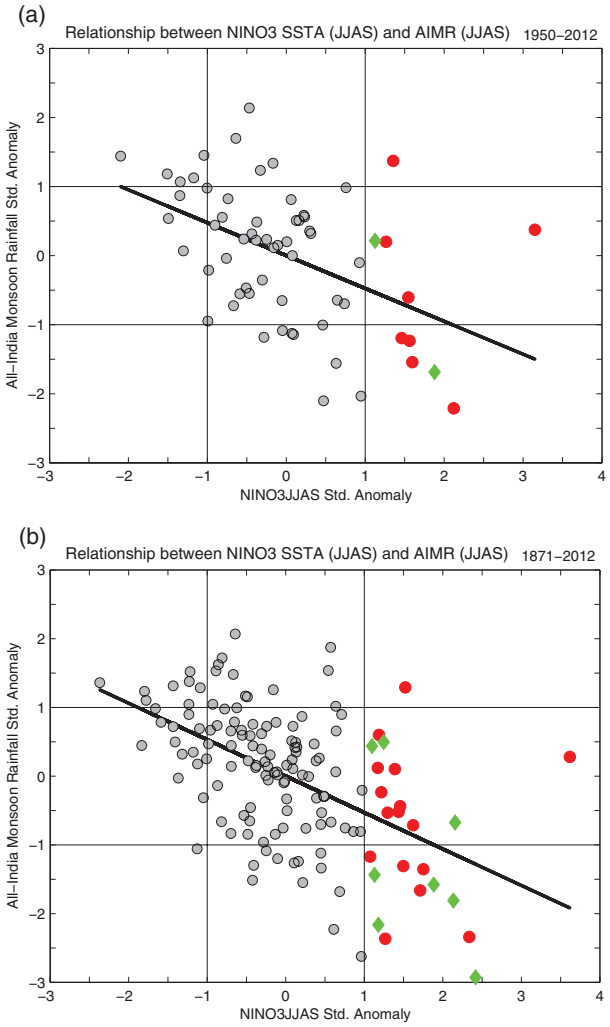

Figure 2. The standardized summer mean (June–September) Niño-3 SST anomaly index and the standardized All-India monsoon rainfall (AIMR) index during (a) the 1950–2012 period and (b) 1871–2012 period. Linear regression of the AIMR index against the Niño-3 index is shown in thick black line. EP and CP El Niño events with standardized Niño-3 SST anomaly index > 1.0 are denoted by red dots and green diamonds, respectively.

with a lower threshold (standardized Niño-3 index exceeding +0.65) (Appendices S1 and S2, Supporting information). These results indicate that the El Niño warming pattern associated with Indian monsoon drought experienced a notable decadal modulation in the late 1970s.

For the purpose of better understanding the underlying physical mechanism, velocity potential anomalies at 200 hPa in response to tropical SST anomalies in strong El Niño years are depicted in Figures 4 and S3. Note that the 200 hPa velocity potential is used as a surrogate for the Walker circulation with negative (positive) anomalies corresponding to ascending (descending) motion anomalies. Corresponding to the aforementioned composite SST difference patterns, composite difference patterns of precipitation and velocity potential at 200 hPa between drought and drought-free El Niño years are featured by enhanced ascending motion

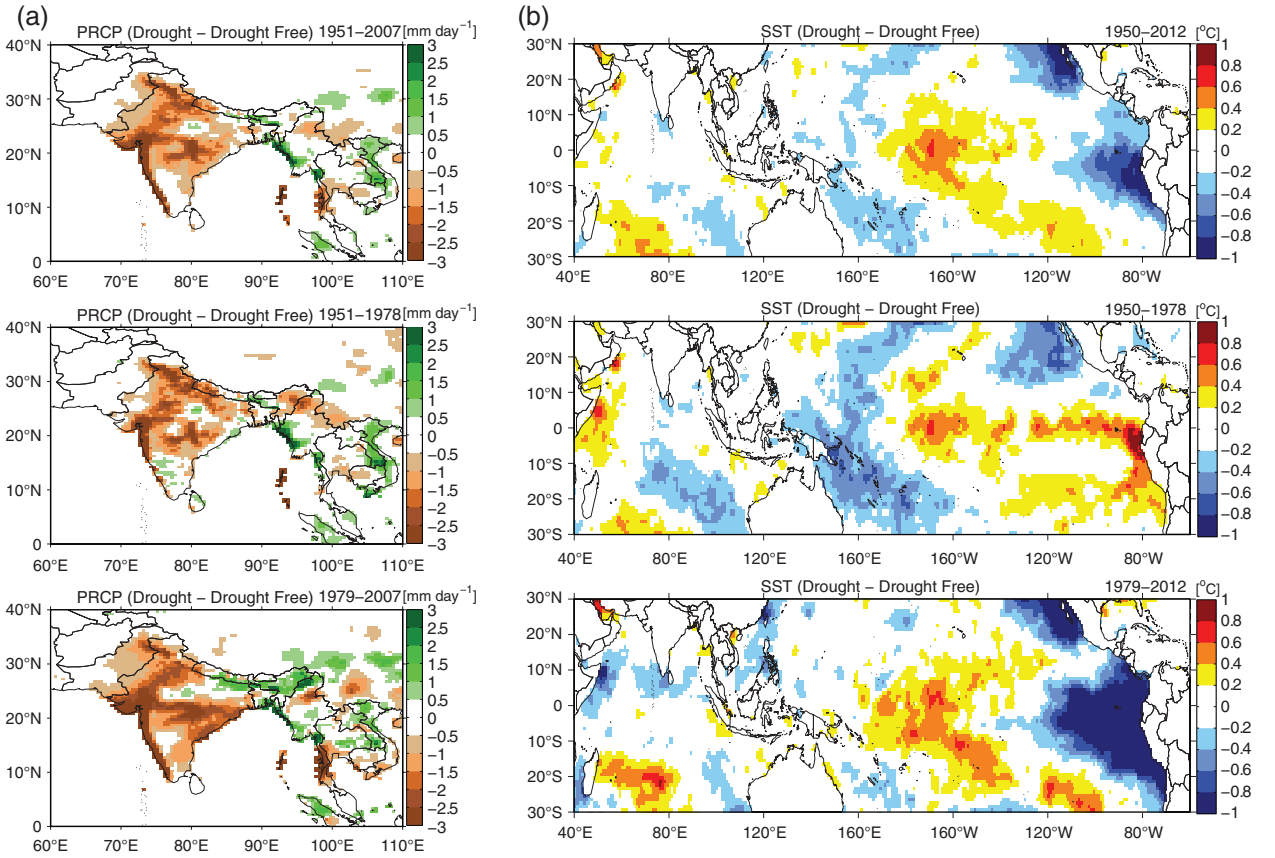

Figure 3. Composite difference patterns of (a) precipitation and (b) SST between drought (standardized AIMR index < -1.0) and drought-free (standardized AIMR index ≥ -1.0) El Niño years during the 1950–2012 period, pre-1979 subperiod and post-1979 subperiod. Precipitation patterns are based on the APHRODITE's precipitation dataset covering the period 1951–2007. SST patterns are based on the HadISST dataset over the 1950–2012 period.

(increased precipitation) in the central Pacific and intensified subsidence (decreased precipitation) over South Asia for both pre-1979 subperiod and post-1979 subperiod (Figure S3). The drought-producing El Niño events in the earlier 1950–1978 subperiod are of typical EP type with positive SST anomalies extended to the date line (e.g. 1972; Figures 4(a) and S4). Although the maximum positive SST anomalies for these typical El Niños lie in the eastern equatorial Pacific, the rising anomalies of the Walker circulation excited by sea surface warming are concentrated in the central equatorial Pacific. Correspondingly, compensatory subsidence anomalies of the Walker circulation are centered over or very close to the Indian subcontinent, leading to suppressed convection and decreased SASM precipitation (Figure 4(f)). Due to the fact that the climatological SST in the central Pacific is higher than that in the eastern Pacific, SST in the central Pacific may exceed the threshold for convection with a relatively small positive SST anomaly, resulting in greater efficiency of CP warming in driving anomalous atmospheric circulation (Graham and Barnett, 1987). It is also worth noting that positive (negative) precipitation anomalies coincide with ascending (descending) motion anomalies, indicating a consistency between convective precipitation changes and large-scale circulation variations in the tropics. Accompanied by more frequent occurrence of the CP type of El Niño after the late 1970s, the drought-producing El Niño events in the later 1979–2012 subperiod may be of traditional EP type with warming extended westward (e.g. 1982; Figure 4(c)) or the newly emerged CP type (e.g. 1987; Figure 4(d)). Both these two types of El Niño warming patterns may lead to the Indian monsoon failure through the atmospheric teleconnection (Figures 4(h) and (i)).

In contrast, the center of anomalous rising motion in drought-free El Niño years shifts to the eastern equatorial Pacific due to the lack of CP warming (e.g. 1976; Figures 4(b) and (g)). Consequently, the anomalous sinking motion shows a prominent southeastward displacement and is centered over the Maritime Continent, leaving the South Asian region less affected by the subsidence anomalies. Despite the fact that the El Niño of 1997 was extremely strong (Niño-3 SST anomaly = 2.40 °C) with positive SST anomalies extended to the date line, the even stronger EP warming effect dominated over the CP warming effect (Figure 4(e)). Accordingly, the centers of anomalous ascending and descending motion were located over the eastern equatorial Pacific and the Maritime Continent, respectively, keeping the Indian monsoon rainfall at a normal state (Figure 4(j)).

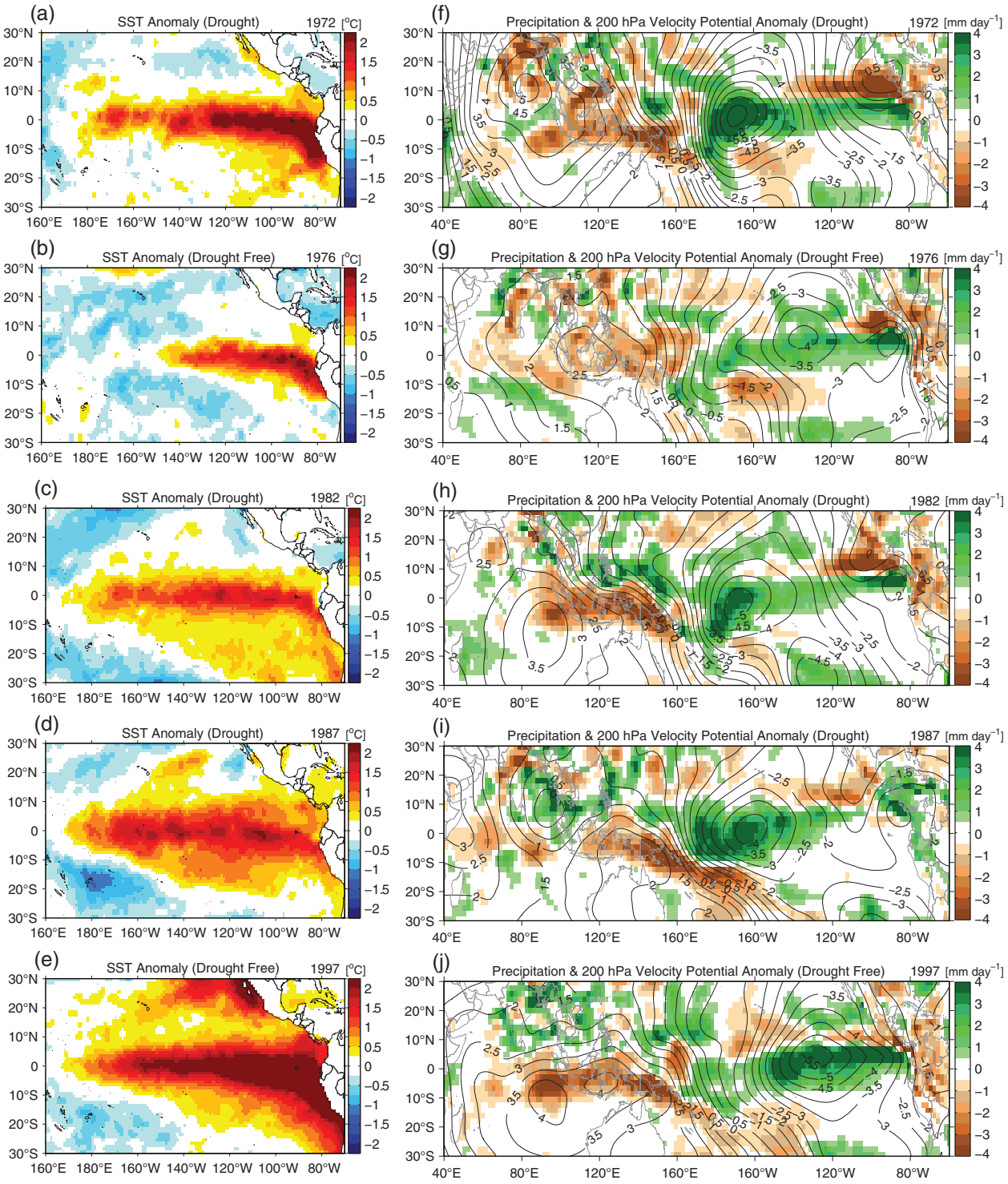

Figure 4. (a)–(e) SST anomalies and (f)–(j) 200 hPa velocity potential anomalies (contours; $\times 10^6$ m^2 s^{-1}) superimposed on precipitation anomalies (shaded) during summer season (June–September) in five strong El Niño years (i.e. 1972, 1976, 1982, 1987 and 1997). Precipitation and velocity potential anomalies are obtained from the Twentieth Century Reanalysis dataset during the 1950–2012 period.

4. Conclusions

We have confirmed that the CP warming plays an essential role in producing Indian monsoon droughts. However, the "flavor" of the drought-inducing El Niño events is not necessarily of the CP type. In the earlier 1950–1978 subperiod, the composite SST difference pattern between drought and drought-free El Niño years is featured by consistently enhanced warming throughout the eastern-to-central equatorial Pacific, and the Indian monsoon drought-inducing El Niño events are of canonical EP type with warming signals extended westward. By contrast, the composite SST difference pattern in the later 1979–2012 subperiod is

characterized by positive SST anomalies in the central Pacific and negative SST anomalies in the eastern Pacific, and the drought-producing El Niño warming pattern may be of traditional EP type or the recently recognized CP type. These findings refine the previous view of drought-producing El Niño warming pattern and raise the possibility that the severe Indian monsoon droughts may be induced by different spatial distributions of El Niño warming associated with climate shifts.

Acknowledgements

This work was supported by the National Natural Science Foundation of China (Grant No. 41405058). Support for the Twentieth Century Reanalysis Project dataset is provided by the U.S. Department of Energy, Office of Science Innovative and Novel Computational Impact on Theory and Experiment (DOE INCITE) program, and Office of Biological and Environmental Research (BER), and by the National Oceanic and Atmospheric Administration Climate Program Office.

Supporting information

The following supporting information is available:

Figure S1. The standardized summer mean (June–September) Niño-3 SST anomaly index and the standardized All-India monsoon rainfall (AIMR) index during the 1950–2012 period. Linear regression of the AIMR index against the Niño-3 index is shown in thick black line. EP and CP El Niño events with standardized Niño-3 SST anomaly index >0.65 are denoted by red dots and green diamonds, respectively.

Figure S2. Composite difference patterns of (a) precipitation and (b) SST between drought (standardized AIMR index <-1.0) and drought-free (standardized AIMR index ≥ -1.0) El Niño (standardized Niño-3 index >0.65) years during the 1950–2012 period, pre-1979 subperiod and post-1979 subperiod.

Figure S3. Composite difference patterns of precipitation (shaded) and velocity potential at 200 hPa (contours; $\times 10^6\ m^2\ s^{-1}$) between drought (standardized AIMR index <-1.0) and drought-free (standardized AIMR index ≥ -1.0) El Niño years during the 1950–2012 period, pre-1979 subperiod and post-1979 subperiod.

Figure S4. (a)–(c) SST anomalies and (d)–(f) 200 hPa velocity potential anomalies (contours; $\times 10^6\ m^2\ s^{-1}$) superimposed on precipitation anomalies (shaded) for summer season (June–September) in drought-producing El Niño years (1951, 1965 and 1972) during the 1950–1978 subperiod.

Figure S5. (a)–(c) SST anomalies and (d)–(f) 200 hPa velocity potential anomalies (contours; $\times 10^6\ m^2\ s^{-1}$) superimposed on precipitation anomalies (shaded) for summer season (June–September) in drought-free El Niño years (1957, 1963 and 1976) during the 1950–1978 subperiod.

Figure S6. (a)–(c) SST anomalies and (d)–(f) 200 hPa velocity potential anomalies (contours; $\times 10^6\ m^2\ s^{-1}$) superimposed on precipitation anomalies (shaded) for summer season (June–September) in drought-producing El Niño years (1982, 1987 and 2009) during the 1979–2012 subperiod.

Figure S7. (a)–(b) SST anomalies and (c)–(d) 200 hPa velocity potential anomalies (contours; $\times 10^6\ m^2\ s^{-1}$) superimposed on precipitation anomalies (shaded) for summer season (June–September) in drought-free El Niño years (1983 and 1997) during the 1979–2012 subperiod.

Table S1. Moderate to strong El Niño events (standardized Niño-3 index >0.65) and the associated All-India monsoon rainfall during the 1950–2012 period. The EP and CP types of El Niño are identified based on the EP/CP ENSO index method developed by Kao and Yu (2009).

Appendix S1. Relationship between El Niño and SASM drought.

Appendix S2. Composite difference patterns.

Appendix S3. Atmospheric responses in drought and drought-free El Niño years.

References

Ashok K, Yamagata T. 2009. The El Niño with a difference. *Nature* **461**: 481–484.

Ashok K, Behera SK, Rao SA, Weng H, Yamagata T. 2007. El Niño Modoki and its possible teleconnection. *Journal of Geophysical Research* **112**: C11007, doi: 10.1029/2006JC003798.

Compo GP, Whitaker JS, Sardeshmukh PD, Matsui N, Allan RJ, Yin X, Gleason BE Jr, Vose RS, Rutledge G, Bessemoulin P, Brönnimann S, Brunet M, Crouthamel RI, Grant AN, Groisman PY, Jones PD, Kruk MC, Kruger AC, Marshall GJ, Maugeri M, Mok HY, Nordli Ø, Ross TF, Trigo RM, Wang XL, Woodruff SD, Worley SJ. 2011. The twentieth century reanalysis project. *Quarterly Journal of the Royal Meteorological Society* **137**: 1–28.

Fan F, Mann ME, Lee S, Evans JL. 2010. Observed and modeled changes in the South Asian summer monsoon over the historical period. *Journal of Climate* **23**: 5193–5205.

Garfinkel CI, Hurwitz MM, Waugh DW, Butler AH. 2013. Are the teleconnections of Central Pacific and Eastern Pacific El Niño distinct in boreal wintertime? *Climate Dynamics* **41**: 1835–1852, doi: 10.1007/s00382-012-1570-2.

Gershunov A, Schneider N, Barnett T. 2001. Low-frequency modulation of the ENSO-Indian monsoon rainfall relationship: signal or noise? *Journal of Climate* **14**: 2486–2492.

Giese BS, Ray S. 2011. El Niño variability in simple ocean data assimilation (SODA), 1871–2008. *Journal of Geophysical Research* **116**: C02024, doi: 10.1029/2010JC006695.

Graham NE, Barnett TP. 1987. Sea surface temperature, surface wind divergence, and convection over tropical oceans. *Science* **238**: 657–659.

Grove RH. 1998. Global impact of the 1789-93 El Niño. *Nature* **393**: 318–319.

Kao H-Y, Yu J-Y. 2009. Contrasting eastern-Pacific and central-Pacific types of ENSO. *Journal of Climate* **22**: 615–632.

Krishna Kumar K, Rajagopalan B, Cane MA. 1999. On the weakening relationship between the Indian monsoon and ENSO. *Science* **284**: 2156–2159.

Krishna Kumar K, Rajagopalan B, Hoerling M, Bates G, Cane M. 2006. Unraveling the mystery of Indian monsoon failure during El Niño. *Science* **314**: 115–119.

Krishnamurthy V, Goswami BN. 2000. Indian monsoon-ENSO relationship on interdecadal timescale. *Journal of Climate* **13**: 579–595.

Kug J-S, Jin F-F, An S-I. 2009. Two types of El Niño events: cold tongue El Niño and warm pool El Niño. *Journal of Climate* **22**: 1499–1515.

Lin R-P, Zhou T-J. 2015. Reproducibility and future projections of the precipitation structure in East Asia in four Chinese GCMs that participated in the CMIP5 experiments. *Chinese Journal of Atmospheric Sciences* **39**(2): 338–356. (in Chinese).

Mantua NJ, Hare SR. 2002. The Pacific Decadal Oscillation. *Journal of Oceanography* **58**: 35–44.

Mehta VM, Lau K-M. 1997. Influence of solar irradiance on the Indian monsoon-ENSO relationship at decadal-multidecadal time scales. *Geophysical Research Letters* **24**: 159–162.

Mooley DA, Parthasarathy B. 1984. Fluctuations in All-India summer monsoon rainfall during 1871-1978. *Climatic Change* **6**: 287–301.

Palmer TN, Branković Č, Viterbo P, Miller MJ. 1992. Modeling interannual variations of summer monsoons. *Journal of Climate* **5**: 399–417.

Parthasarathy B, Munot AA, Kothawale DR. 1994. All-India monthly and seasonal rainfall series: 1871-1993. *Theoretical and Applied Climatology* **49**: 217–224.

Parthasarathy B, Munot AA, Kothawale DR. 1995. Monthly and seasonal rainfall series for all India, homogeneous regions and meteorological subdivisions: 1871-1994. Research Report No. RR-065, 113 pp. [Available from Indian Institute of Tropical Meteorology, Homi Bhabha Road, Pune 411008, India.]

Rasmusson EM, Carpenter TH. 1983. The relationship between eastern equatorial Pacific sea surface temperatures and rainfall over India and Sri Lanka. *Monthly Weather Review* **111**: 517–528.

Rayner NA, Parker DE, Horton EB, Folland CK, Alexander LV, Rowell DP, Kent EC, Kaplan A. 2003. Global analyses of sea surface temperature, sea ice, and night marine air temperature since the late nineteenth century. *Journal of Geophysical Research* **108**(D14): 4407, doi: 10.1029/2002JD002670.

Ropelewski CF, Halpert MS. 1987. Global and regional scale precipitation patterns associated with the El Niño/Southern Oscillation. *Monthly Weather Review* **115**: 1606–1626.

Trenberth KE. 1990. Recent observed interdecadal climate changes in the Northern Hemisphere. *Bulletin of the American Meteorological Society* **71**: 988–993.

Wang B, Wu R, Fu X. 2000. Pacific–East Asian teleconnection: how does ENSO affect East Asian climate? *Journal of Climate* **13**: 1517–1536.

Wang B, Wu R, Lau K-M. 2001. Interannual variability of the Asian summer monsoon: contrasts between the Indian and the western North Pacific-East Asian monsoons. *Journal of Climate* **14**: 4073–4090.

Webster PJ, Yang S. 1992. Monsoon and ENSO: selectively interactive systems. *Quarterly Journal of the Royal Meteorological Society* **118**: 877–926.

Yatagai A, Kamiguchi K, Arakawa O, Hamada A, Yasutomi N, Kitoh A. 2012. APHRODITE: constructing a long-term daily gridded precipitation dataset for Asia based on a dense network of rain gauges. *Bulletin of the American Meteorological Society* **93**: 1401–1415, doi: 10.1175/BAMS-D-11-00122.1.

Yu J-Y, Kao H-Y. 2007. Decadal changes of ENSO persistence barrier in SST and ocean heat content indices: 1958-2001. *Journal of Geophysical Research* **112**: D13106, doi: 10.1029/2006JD007654.

Yu J-Y, Zou Y, Kim ST, Lee T. 2012. The changing impact of El Niño on US winter temperatures. *Geophysical Research Letters* **39**: L15702, doi: 10.1029/2012GL052483.

Zheng F, Fang X-H, Yu J-Y, Zhu J. 2014. Asymmetry of the Bjerknes positive feedback between the two types of El Niño. *Geophysical Research Letters* **41**: 7651–7657, doi: 10.1002/2014GL062125.